Optica Applicata, Vol. XLVII, No. 2, 2017
DOI: 10.5277/oa170201

Enlarging the bandwidth of a two-dimensional photonic crystal mirror in the visible range

IVAN VOZNYUK[1, 2*], SALIM BOUTAMI[1, 2], ALAIN GLIÈRE[1, 2]

[1]Université Grenoble Alpes, F-38000 Grenoble, France

[2]CEA, LETI, MINATEC Campus, F-38054 Grenoble, France

[*]Corresponding author: ivan.voznyuk@bk.ru

The spectral properties of reflective mirrors based on a classic design of two-dimensional subwavelength photonic crystal are investigated numerically in the visible wavelength range. These reflectors are meant to be made of silica and silicon nitride. A novel numerical strategy is proposed in order to determine the optimal value of the grating fill factor yielding an efficient level of reflectance through the maximal range of wavelengths.

Keywords: diffraction gratings, subwavelength structures, resonators.

1. Introduction

Number of studies in the domain of photonic devices is rapidly growing, which means that the interaction of light with periodic structures and resonant photonic elements is of a great scientific and technological interest. Bragg mirrors have been extensively used during decades for the realization of devices such as Fabry–Pérot filters [1, 2] or vertical cavity surface emitting lasers (VCSEL) [3]. In the infrared domain, these mirrors have been recently replaced by one and 2D resonant gratings [4–10]. Such gratings have shown to be highly reflective, within a single layer, which is beneficial in terms of compactness and cost of devices, with an additional advantage of polarization control of VCSELs for example [3, 11].

In the infrared range, the available transparent materials may show high refractive index contrast, which enables very broadband mirrors [6]. In the visible range, however, transparent dielectric materials have much lower index contrast, which makes it difficult to realize broadband grating mirrors. It becomes thus essential to work on the multimodal behavior of the grating to obtain a relatively broad reflectance peak.

In this paper, the attention is focalized on a classic design of 2D gratings made of silica/silicon nitride, which are commonly used in microelectronics, and are transpar-

ent in the whole visible range. The geometry related to the investigated configurations is of a 90° rotational symmetry and, thus, independent of the incident light polarization.

Here, we report a new numerical strategy of a choice of the grating parameters enabling to enlarge the spectral reflectivity. The proposed strategy is based on the fine tuning of modal resonances. For simplicity and clarity, the discussion is limited to an example with only one parameter to be optimized, which is the fill factor related to the resonant grating.

2. Configuration of a 2D resonant grating

Figure 1 schematically illustrates a model of 2D resonant reflector studied in this work. The grating parameters are the period, grating thickness, fill factors and the materials refractive indices. A regular array of cylindrical pillars, made of silicon nitride, embedded into a silica substrate, is considered. The superstrate is air. Normal incidence of the wave impinging from the substrate side on the grating is assumed.

We limit ourselves to the case of a grating with a 90° rotational symmetry, *i.e.*, in which the periods related to both *x* and *y* directions are equal. Thus, the spectral response of the device in normal incidence is the same for TE and TM polarizations. The calculations are done with the Comsol Multiphysics commercial package (COMSOL AB, Sweden), based on the finite element method (FEM). Periodic boundary conditions are applied on both lateral sides of the domain, and perfectly matched layers allow limiting the computational domain on top and bottom sides.

Among three main grating parameters, the only fill factor is varying in the present work. Two remaining parameters, the grating period Λ and the grating thickness d are fixed to 270 and 125 nm throughout all the calculations.

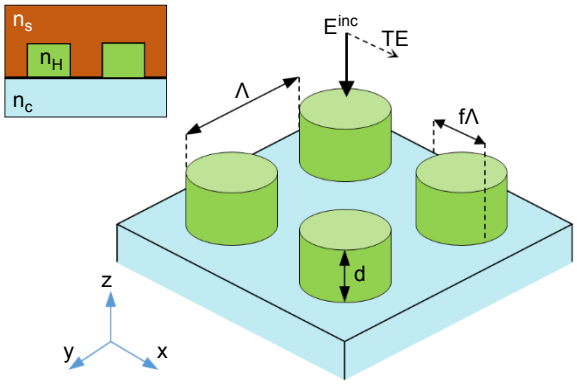

Fig. 1. Model of the 2D resonant reflector made of cylindrical pillars of silicon nitride. The parameters are the grating period Λ, the grating thickness d and the silicon nitride fill factor f, yielding the diameter of the pillars $w = f\Lambda$. The inset is a cross-section through the diameter of the pillars along the x or y axis. The substrate and surrounding medium of the silicon nitride pillars ($n_H = n_{SiN} = 2.0$) is silica ($n_s = n_{SiO_2} = 1.5$). The superstrate is air ($n_c = n_{air} = 1.0$).

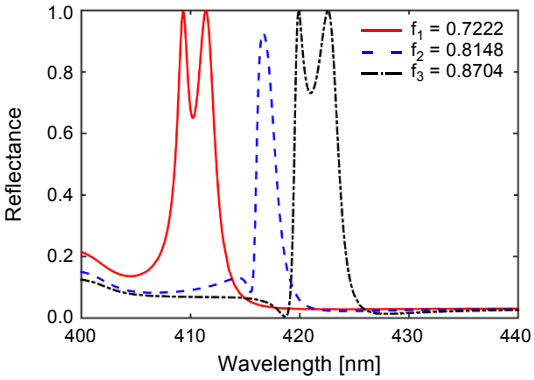

Fig. 2. Spectral response simulated *versus* wavelength for the 2D resonance grating array with cylindrical pillars corresponding to the period $\Lambda = 270$ nm, thickness $d = 125$ nm, and fill factors $f_1 = 0.7222$, $f_2 = 0.8148$, and $f_3 = 0.8704$.

It is worth mentioning that the ratio between these parameters is of the prime importance. For example, they set the grating array resonances in the desired wavelength range, and getting symmetric Fano-resonance peaks, *i.e.*, background reflection of the effective index layer close to zero [12]. Nevertheless, they do not change the proposed numerical strategy, presented in this paper.

3. Three regimes detected

Figure 2 illustrates the spectral response of the 2D mirror presented above with pillars of three different values of fill factors.

An interesting phenomenon is observed: depending on the fill factor, the grating can show one or two peaks of reflectance. More precisely, by increasing the fill factor, one gets two peaks of reflectance, passing by a situation of a single reflectance peak (Fig. 2). In order to understand the nature of these peaks, maps of the scattered electric field modulus $|E^{sc}|$ at the wavelengths of the peaks corresponding to the same fill factors are plotted in Fig. 3.

Starting with the case corresponding to the fill factor $f = f_1$, it can be noted that the two peaks correspond to different distributions of the electromagnetic field (Figs. 3**a** and 3**b**). For the case of fill factor $f = f_2$, a single peak is observed (Fig. 2). As can be seen from this figure, this peak does not reach the level of total reflectance as the previous ones. A map of electric field modulus related to this peak can be viewed in Fig. 3**c**. It can be noted, that this map is quite similar to the second one from the previous case. Finally, increasing the fill factor up to $f = f_3$, two peaks reaching total reflectance can be observed again.

Some interesting phenomena appear when comparing the results corresponding to the fill factors $f = f_1$ and $f = f_3$. On the one hand, it can be noted that by increasing the fill factor, the electric field map related to the second peak for fill factor f_1 (Fig. 3**b**)

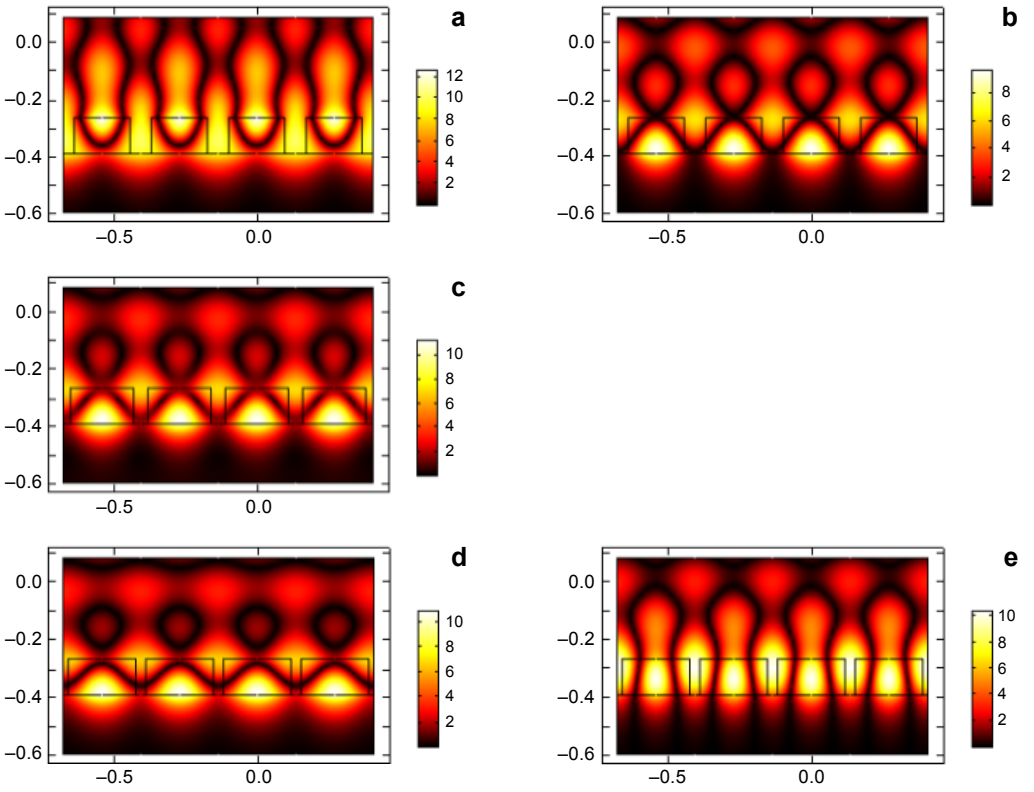

Fig. 3. Maps of the electric scattered field modulus $|E^{sc}|$ in the middle cross-section of pillars containing the electric field vector. Two peaks are obtained for the fill factor f_1 at wavelengths $\lambda = 409.3$ nm (**a**) and $\lambda = 411.4$ nm (**b**). A single peak of reflectance is obtained for f_2 at $\lambda = 416.7$ nm (**c**). Two peaks are obtained for fill factor f_3 at $\lambda = 419.9$ nm (**d**) and $\lambda = 422.6$ nm (**e**).

is similar to the electric field related to the first peak for fill factor f_3 (Fig. 3**e**). On the other hand, the electric field related to the first peak for fill factor f_1 presented (Fig. 3**a**) is rather different from the electric field related to the second peak for fill factor f_2 (Fig. 3**e**).

In order to understand the nature of these phenomena and describe the behavior of the reflectance peaks, the spectral positions of the peaks, as well as the minimum between them, are examined for values of the fill factor varying from 0.6 to 0.9.

These three characteristic features are determined using a metamodel, based on a radial basis functions decomposition [13, 14], in order to improve computational efficiency. The reflectance spectrum is iteratively refined by simulating new points at positions where the metamodel exhibits changes in gradient sign. Figure 4 provides a view of the behavior of these characteristics through the chosen range of fill factors. Three regimes clearly appear.

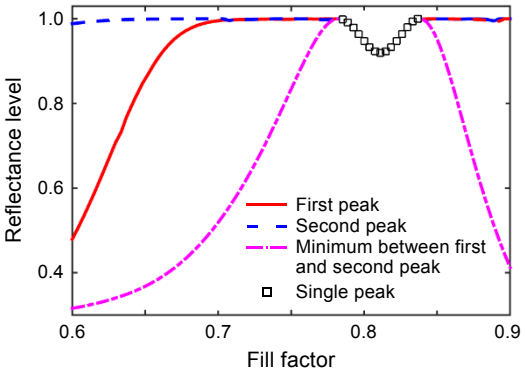

Fig. 4. Level of calculated reflectance related to the first peak, second peak and minimum between them calculated for the fill factor varying from 0.6 to 0.9. The region where a single peak exists is presented as well.

First regime: two peaks existing. The first regime shows the existence of two peaks. We remind that these peaks correspond to different distributions of the electromagnetic field, presented in Figs. 3**a** and 3**b**. Both of them are red-shifted when the fill factor is increased. As can be seen from Fig. 4, the second peak quickly reaches the level of total reflectance, while the first one is reaching it slower. As the peaks both get high level of reflectance, they get spectrally closer to each other, and thus the reflectance at the minimum between them also increases.

Second regime: a single peak. The second regime begins when the minimum between the two peaks reaches the level of the total reflectance, as can be seen in Fig. 4. The main criterion of the second regime is that a single peak exists. This peak is not holding on the level of total reflectance: it first decreases to around 90%, and then starts growing again.

Third regime: two peaks crossed each other. The third regime corresponds to the reappearance of two peaks reaching the total reflectance level, with a distinctive minimum between them. These two peaks are red-shifted when the fill factor is increased. The mapping of the electric field related to the second peak corresponds to the first peak of first regime. In order to confirm and formalize such behavior, the wavelength positions of the two peaks are plotted in the same range of the fill factors (solid lines in Fig. 5).

As can be seen, the first peak is red-shifted faster than the second peak. After passing through the second regime, the first peak outruns the second one and their positions become inverted.

The band structure of the grating has been calculated by the FEM, and the spectral positions of the actual grating modes have been extracted, which obviously do not correspond to the reflectance maxima (Fig. 5). It can be seen that, although the reflectance peaks cross each other (solid lines), the related modes do not (dashed lines), and we

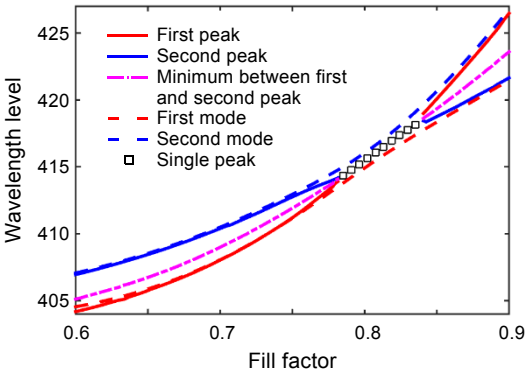

Fig. 5. Evolution of the simulated wavelength corresponding to the first and second peaks and the minimum between them. The first and second modes, contouring the peaks trajectories, are also plotted. The region where a single peak exists is presented as well.

observe an anticrossing between them, which explains why the field map of the second peak in first regime is similar to the field map of the first peak in third regime. The first peak in first regime does transform into the second peak in third regime, but the electric field distribution is much more altered, which is correlated with the higher wavelength dependence of mode with fill factor. Indeed, the wavelength of resonance is related to light distribution between high and low refractive indices. For the map field which remains similar in all three regimes, the energy is changing almost linearly, due solely to geometric increase of pillars with fill factor. For the other one, the field distribution is more disturbed, and the wavelength increases faster.

4. Proposed numerical strategy

In order to obtain a grating that would yield a large spectrum of reflectance, another parameter, that is the spectral distance between the reflection peaks, should be taken into account (Fig. 6).

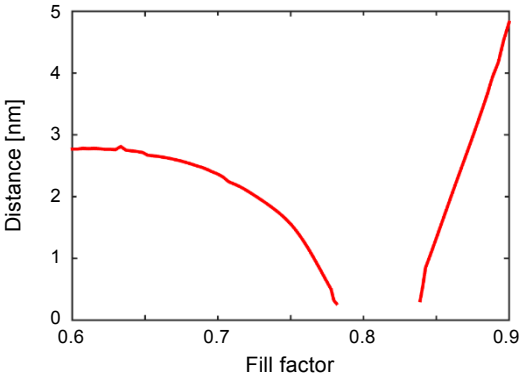

Fig. 6. Evolution of the spectral distance between the two peaks present in the first and third regimes.

The necessity of treating both peaks of reflectance is clear now: it allows us to bring them closer in order to obtain a broader reflection spectrum. Besides, introducing a third parameter, *i.e.*, the minimum between the peaks, allows us to determine the parameters for which the resonant grating would have the maximal spectral range for a given level of minimal reflectance.

Thus, the 2-steps strategy of an optimal fill factor definition proposed in this paper is the following:

– First, using Fig. 4, one has to determine the fill factors yielding the demanded level of reflectance for the minimum between the two peaks.

– Second, with the help of Fig. 6, one has to choose one among the two values obtained at the previous step, yielding the maximal spectral peak distance.

As an example, two optimal gratings are determined, which respectively reach reflectance levels higher than 90% and 99%. The spectral responses corresponding to these grating reflectors are plotted in Fig. 7. The resulting peaks are respectively 3.5 and 5.7 times wider than the ones presented in Fig. 2.

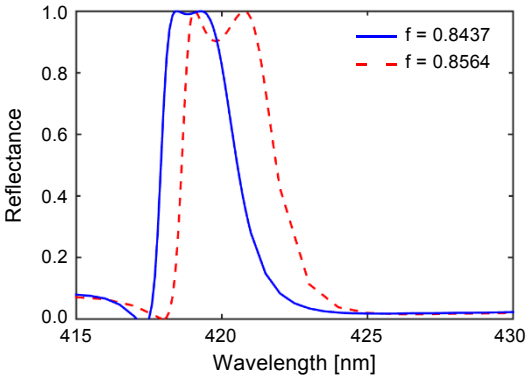

Fig. 7. The spectral response of the 2D grating composed of cylindrical pillars of fill factors $f = 0.8564$ and $f = 0.8437$, optimally chosen in order to get reflectance higher than 90% and 99% through the maximal range of wavelengths.

In summary, a novel numerical strategy has been introduced to design broader band reflection grating in the visible light range. Getting in the comprehension of the modal behavior of a 2D resonant grating with cylindrical pillars, the proposed technique allows determining the device parameters yielding the maximal spectral width for a given level of reflectance. As a result, two values of fill factor are proposed in order to design the resonant reflectors, providing a reflection bandwidth of ~2.37 and ~1.16 nm with $R > 90\%$ and $R > 99\%$, respectively, around $\lambda = 420$ nm.

5. Conclusion

It is worth mentioning that the present gratings were designed to operate around 420 nm, but the investigated idea can be used in the entire visible range of wavelength, by sim-

ply applying a scaling rule on both height and period, considering that refractive indices of the material used do not change much with wavelength.

Such wider-bandwidth mirrors could be integrated in photonic devices operating in the visible range, such as resonant cavity light emitting diodes for example.

References

[1] MATEUS C.F.R., HUANG M.C.Y., LU CHEN, CHANG-HASNAIN C.J., SUZUKI Y., *Broad-band mirror (1.12–1.62 μm) using a subwavelength grating*, IEEE Photonics Technology Letters **16**(7), 2004, pp. 1676–1678.

[2] MATEUS C.F.R., HUANG M.C.Y., YUNFEI DENG, NEUREUTHER A.R., CHANG-HASNAIN C.J., *Ultrabroad-band mirror using low-index cladded subwavelength grating*, IEEE Photonics Technology Letters **16**(2), 2004, pp. 518–520.

[3] HUANG M.C.Y., ZHOU Y., CHANG-HASNAIN C.J., *A surface-emitting laser incorporating a high-index -contrast subwavelength grating*, Nature Photonics **1**(2), 2007, pp. 119–122.

[4] LIU Z.S., TIBULEAC S., SHIN D., YOUNG P.P., MAGNUSSON R., *High-efficiency guided-mode resonance filter*, Optics Letters **23**(19), 1998, pp. 1556–1558.

[5] DING Y., MAGNUSSON R., *Resonant leaky-mode spectral-band engineering and device applications*, Optics Express **12**(23), 2004, pp. 5661–5674.

[6] BOUTAMI S., BAKIR B.B., HATTORI H., LETARTRE X., LECLERCQ J.-L., ROJO-ROMEO P., GARRIGUES M., SEASSAL C., VIKTOROVITCH P., *Broadband and compact 2-D photonic crystal reflectors with controllable polarization dependence*, IEEE Photonics Technology Letters **18**(7), 2006, pp. 835–837.

[7] JIANYONG MA, SHIJIE LIU, DAWEI ZHANG, JIANKE YAO, CHEN XU, JIANDA SHAO, YUNXIA JIN, ZHENGXIU FAN, *Transmission guided-mode resonance filters based on high reflection multilayer stacks*, Optik – International Journal for Light and Electron Optics **121**(12), 2010, pp. 1144–1147.

[8] MAGNUSSON R., SHOKOOH-SAREMI M., *Physical basis for wideband resonant reflectors*, Optics Express **16**(5), 2008, pp. 3456–3462.

[9] SHOKOOH-SAREMI M., MAGNUSSON R., *Properties of two-dimensional resonant reflectors with zero -contrast gratings*, Optics Letters **39**(24), 2014, pp. 6958–6961.

[10] MAGNUSSON R., *Wideband reflectors with zero-contrast gratings*, Optics Letters **39**(15), 2014, pp. 4337–4340.

[11] BOUTAMI S., BENBAKIR B., LECLERCQ J.-L., VIKTOROVITCH P., *Compact and polarization controlled 1.55 μm vertical-cavity surface-emitting laser using single-layer photonic crystal mirror*, Applied Physics Letters **91**(7), 2007, article ID 071105.

[12] MÅRTENSSON N., WEINELT M., KARIS O., MAGNUSON M., WASSDAHL N., NILSSON A., STÖHR J., SAMANT M., *Coherent and incoherent processes in resonant photoemission*, Applied Physics A **65**(2), 1997, pp. 159–167.

[13] BROOMHEAD D.S., LOWE D., *Radial Basis Functions, Multi-Variable Functional Interpolation and Adaptive Networks*, Royal Signals and Radar Establishment, 1988.

[14] BUHMANN M.D., *Radial Basis Functions: Theory and Implementations*, Cambridge University Press, 2003.

Received August 10, 2016
in revised form October 10, 2016